



Oxidation of isopropanol and acetone adsorbed on TiO₂ under plasma generated ozone flow: Gas phase and adsorbed species monitoring



C. Barakat ^{a,*}, P. Gravejat ^{b,c}, O. Guaitella ^a, F. Thevenet ^{b,c}, A. Rousseau ^a

^a LPP, Ecole Polytechnique, UPMC, Université Paris Sud 11, CNRS, Palaiseau, France

^b Université Lille Nord-de-France, F-59000 Lille, France

^c Mines Douai, CE, F-59508 Douai, France

ARTICLE INFO

Article history:

Received 24 June 2013

Received in revised form 27 August 2013

Accepted 6 September 2013

Available online 13 September 2013

Keywords:

Ozone

Dielectric barrier discharge (DBD)

Post plasma catalysis

Volatile organic compound (VOC)

Adsorbent

ABSTRACT

The regeneration of isopropanol (IPA) and/or acetone saturated TiO₂ surface by ozone is investigated. TiO₂ catalyst is placed downstream a dielectric barrier discharge and is subsequently exposed to ozone considered as the main oxidative species generated by non-thermal plasma and able to interact with the material surface at room temperature. The oxidation of isopropanol and/or acetone is monitored using two parallel and complementary infrared diagnostics: (1) Fourier Transform Infrared Spectroscopy for the analysis of the gas phase composition; and (2) Diffuse Reflectance Infrared Fourier Transform Spectroscopy for the in situ analysis of the adsorbent/catalyst surface. In this study, the pollutant is first adsorbed on the TiO₂ surface, the plasma being switched off. The irreversibly adsorbed amounts of isopropanol and acetone have been respectively quantified as 5.3 μmol/m² and 1.9 μmol/m². In a second step, the plasma is switched on to regenerate the surface by mineralization of the adsorbed organic species. A 70-min plasma phase, with approximately 20 ppm of ozone constantly flowing through the adsorbent bed yields 8.5 nmol and 8.9 nmol of CO₂ per injected joule of energy for isopropanol and acetone saturated surfaces, respectively. Acetone has been evidenced as the main oxidation intermediate of isopropanol on TiO₂ surface. It has been proven that the complete oxidation of isopropanol and acetone is mainly limited by the acetone oxidation rate. Competitive adsorption on the surface of the catalyst between both compounds has been studied. Results obtained are compared with those observed in the photocatalytic oxidation of the same species.

© 2013 Elsevier B.V. All rights reserved.

1. Introduction

The emission of volatile organic compounds (VOCs) by various materials is an important source of indoor air pollution and can be a threat to human health. With 80% of our time spent indoors as well as an increasing need of highly pure atmospheres for specific industrial activities (pharmaceutical, aerospace, microelectronics) [1], it has recently become of great concern in many European countries to limit the emissions of volatile organic compounds and odors present in confined environments [2].

For the abatement of dilute VOCs, with concentrations hardly exceeding 100 ppb, conventional techniques like thermal and thermocatalytical oxidation are not suitable, mainly due to their high-energy consumption [3]. The treatment of polluted air streams containing VOCs by non-thermal plasma (NTP) is an alternative to

conventional techniques, especially for low hydrocarbon concentrations.

The specific advantage of NTP is the production of energetic electrons without heating the gas [4,5]. There are two widely used methods for generating non-thermal plasmas at atmospheric pressure, namely corona discharges and dielectric barrier discharges (DBDs) [4,5]. Corona discharges have many applications in industry, where relatively small concentrations of excited or charged species are needed (electrostatic precipitators, copying machines, etc.) [5]. On the other hand, DBDs are used for applications of large volume plasma chemistry at atmospheric pressure [5]. They combine the advantages of non-equilibrium plasma properties (high reactivity at ambient temperature) with the ease of atmospheric-pressure operation [5]. A prominent feature is the simple scalability from small laboratory reactors to large industrial installations with megawatt input powers [5]. Barrier discharges are characterized by the presence of at least one insulating layer, the dielectric barrier, between two planar or cylindrical electrodes, which requires alternative voltages for their operation; the dielectric, being an insulator, cannot pass a dc current. In DBDs, the formation of electric arcs is avoided due to the presence of the

* Corresponding author at: Laboratoire de Physique des Plasmas, Ecole Polytechnique route de Saclay, 91128 Palaiseau Cedex, France. Tel.: +33 1 69 33 58 86; fax: +33 1 69 33 58 61.

E-mail address: christelle.barakat@lpp.polytechnique.fr (C. Barakat).

dielectric between the two electrodes. The dielectric barrier distributes the micro-discharges throughout the discharge volume initiating the chemical reactions by reactive species like ions, radicals and activated molecules [4–8].

Regarding VOC abatement, the main drawback of NTP is an incomplete oxidation of the targeted compounds leading to partially oxidized and possibly toxic by-products [9,10]. This can be overcome by coupling non-thermal plasma with catalytic and/or photocatalytic sorbents [11,12]. This coupling technique has proven to be efficient for VOC removal at room temperature. The plasma technology in the form of a DBD coupled to a catalyst enables high oxidation efficiency and the *in situ* regeneration of the catalyst's surface by (i) mineralizing the adsorbed VOCs, and (ii) restoring the oxidation surface state. The coupling of plasma with the catalyst also enables a better control of the surface oxidation state by increasing the oxidation rate and eliminating by-product poisoning at lower energy cost [13–16]. The combination of NTP with a catalyst can be either single stage, with the catalyst inserted directly inside the discharge zone, or two-stage, with the catalyst placed downstream the NTP reactor [11,17,18]. Coupling mechanisms involved in this plasma-catalyst synergy have not been fully understood and little is known about the role of the different plasma generated species involved in the oxidation improvement.

In this work, a two-stage system is used in order to understand the ozone contribution in the plasma/catalyst interaction process. Considering a DBD ignited in air, ozone is the primary long lived oxidative species able to reach the catalyst's bed, placed downstream the discharge. This approach allows the distinction of the ozonation effect from the real synergetic effect between NTP and catalysis in a packed bed reactor configuration. Another prominent feature of the system is that the plasma is not turned on continuously; it is sequentially turned on after the breakthrough of the pollutant on the catalyst/adsorbent surface, thus reducing the energy consumption further.

In this study, titanium dioxide (TiO_2) is used as a sorbent and catalyst. Numerous studies [19,20] have been performed on TiO_2 , namely for its high photocatalytic activity and its high oxidation potential on many organic compounds [21]. Several works have been conducted to show the synergetic effect of plasma/ TiO_2 systems but the oxidation mechanisms are still not well understood [22] and the contributions of the different species involved (UV, lattice oxygen, molecularly adsorbed oxygen species, electron oxidizing species with short or long lifetimes, etc.) are not clearly defined. As Guaitella et al. showed [22], the photocatalytic activity of TiO_2 is negligible in the plasma except if additional UV lamps are used to activate the solid. This work enables to distinguish the role of a main long lifetime species, ozone, generated by the plasma and its interaction with TiO_2 . Studies conducted by Arsac et al. [23,24] show the photocatalytic effect of TiO_2 in the oxidation of a model VOC where different active oxygen containing species are responsible for the oxidation processes. A distinction between the ozone effect and the UV effect is an important step in understanding the synergy observed in plasma-photocatalysis systems.

The two organic compounds studied are isopropanol (IPA) and acetone. As they are commonly used as solvents and have a low molecular weight, they are interesting to study because of their limited number of reaction intermediates and by-products, hence simplifying and clarifying the diagnosis. Moreover, acetone has been reported as the main intermediate in the oxidation of IPA into CO_2 and H_2O [23–26]. The oxidation of these two model VOCs is well described in literature, mainly in photocatalysis, and is hence a good basis for comparing and understanding what happens under plasma generated ozone flow.

In order to investigate the heterogeneous oxidation pathways of isopropanol and acetone onto TiO_2 surface, both adsorbed and gas phase characterizations are performed. The *in situ* surface analysis

of the adsorbent/catalyst using DRIFTS (Diffuse Reflectance Infrared Fourier Transform Spectroscopy) and the gas phase characterization using FTIR (Fourier Transform Infrared Spectroscopy) enable the study of the surface oxidation mechanisms and catalyst regeneration.

2. Experimental setups

Two experimental setups have been used in this study. They are both structured alike: (i) gas flow preparation, (ii) plasma reactor, (iii) sorbent/catalyst bed and (iv) infrared diagnosis. Schemes of both experimental setups are reported in Fig. 1. They mainly differ by the nature of their infrared diagnosis. The first setup (Fig. 1a) is equipped with a Fourier Transform Infrared spectrometer (FTIR) dedicated to the gas phase analysis; the second experimental setup (Fig. 1b) is equipped with a Diffuse Reflectance Infrared Fourier Transform Spectrometer (DRIFTS) devoted to the adsorbed phase characterization.

2.1. Gas flow preparation and materials

The two model organic compounds used in this study are 2-Propanol (34959 – CHROMASOLV®, for HPLC, absolute, 99.9%) and acetone (270725 – CHROMASOLV®, for HPLC, $\geq 99.9\%$) both prepared by Sigma-Aldrich.

Certified gas cylinders are supplied by Air Liquide. The regulation of the gas flow is insured using Brooks mass flow controllers. Synthetic air, oxygen and argon cylinders are used to prepare the carrier gas flow. For experiments dedicated to the gas phase characterization (Fig. 1a), the main gas flow consists of synthetic air (alphagaz 1). For experiments dedicated to the adsorbed phase monitoring (Fig. 1b), the main gas flow consists in 20% oxygen (alphagaz 1) balanced in argon (alphagaz 2). The reason for not using nitrogen during DRIFTS experiments is the possible accumulation of nitrogen oxides (NOx) on TiO_2 surface generated by the upstream DBD. Indeed, the NOx concentration generated during plasma in the gas phase is below the FTIR detection limits (ca. 10 ppb); however, NOx may progressively accumulate on TiO_2 surface. Due to their high cross section, they may lead to intense parasite peaks in adsorbed phase experiments. Depending on the experimental setup, IPA or acetone is diluted in air or the O_2/Ar mixture according to their partial pressure using a saturator/condenser system placed in a cryostat for temperature regulation, as shown in Fig. 1.

The humidity level in the synthetic air flow was less than 3 ppm which corresponds to a level of 0.01% of relative humidity at 25 °C. Based on the works of Sivanchandiran et al. [27], the IPA quantity adsorbed is not affected by the 0.01% humidity level. Sivanchandiran et al. [27] also state that below 35% relative humidity, the presence of hydroxyl groups on the surface as well as water molecules in the gas phase does not play a significant role in the mineralization process.

The material used as sorbent and catalyst consists in P25 Degussa Aerioxide TiO_2 powder with a specific surface of 45 m²/g. The mass of TiO_2 used in the gas phase monitoring experimental setup is 200 mg. In the case of the adsorbed phase characterization setup, approximately 6 mg of TiO_2 are used.

2.2. Dielectric barrier discharge reactor

Two similar DBD reactors are designed for gas phase and adsorbed phase experiments.

- The plasma reactor of the gas phase characterization system consists of a Pyrex glass tube of 5.8 mm inner diameter, 8 mm outside

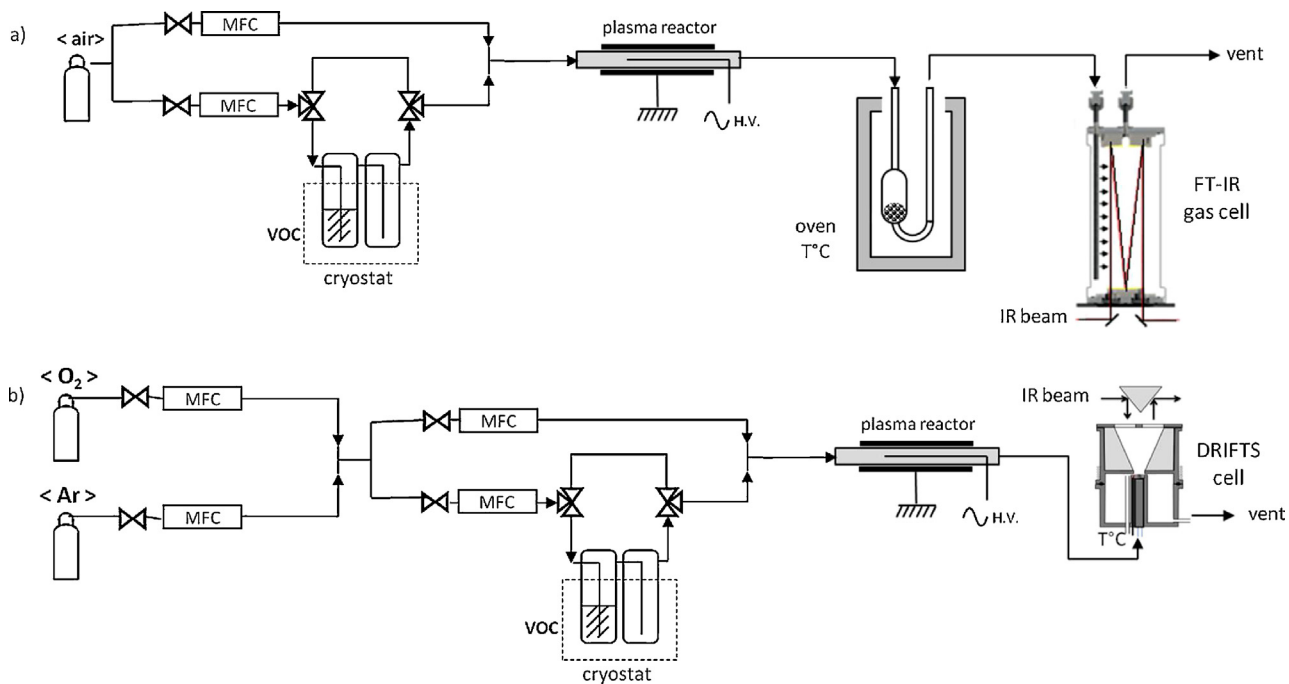


Fig. 1. Schemes of the experimental setups: (a) gas phase studies using FTIR analysis and (b) surface studies using DRIFTS analysis.

diameter and 20 cm length. The inner electrode consists of a copper sheet of 3.1 mm width stuck onto the inner surface of the tube. The outer electrode is an 18 mm long copper sheet stuck on the outer surface of the tube.

- In the adsorbed phase monitoring apparatus, the inner electrode consists of an 80 μ m thick tungsten wire and the outer electrode is a 5 cm wide copper sheet wrapped around the reactor. The dielectric is a Pyrex glass tube with 2.1 mm thickness and 1.4 mm inner diameter.

When the plasma is turned on, the first species created are charged species: electrons, positive and negative ions (O_2^+ , O^- , O_2^- , N^+ , N_2^+), and excited states. The lifetime of these species is very short and ranges between 1 and 100 μ s [28]. Thus, after a few milliseconds, the only remaining species are ozone (O_3) and nitrogen oxides (NO , N_2O , NO_2 , NO_3 , N_2O_5) characterized by lifetimes exceeding several hours [28]. The typical transition time for the gas between reactors outlet and TiO_2 bed has been calculated as 2.5 ms. The only species able to interact with TiO_2 surface are the long lived species, i.e. NO_x and ozone molecules. The two reactors are designed for generating dielectric barrier discharges with low frequency sinusoidal power supply (50 Hz and 200 Hz) at relatively low voltage (below 10 kV) and the residence time of the gas flowing through the plasma zone is constant, ca. 1 ms in both reactors.

The critical parameter to control the ozone concentration with a constant gas flow is the injected power, which is calculated using the Lissajous figure method well known as "Manley method" [29,30]. A measurement capacitance (C_m) of 680 pF is placed in series with the DBD reactors. The applied voltage and voltage on C_m are measured using two high voltage probes (PPE20 kV Lecroy), and are monitored using a 600 MHz LeCroy oscilloscope. The transferred charges measured on C_m are plotted as a function of voltage applied onto the reactor to obtain the average power injected during one discharge cycle by integrating the area of the characteristic Lissajous figure. Fig. 2 shows ozone produced by both non-thermal plasma setups used, as a function of the specific input energy expressed in J/L. The specific input energy is the ratio of the injected power over the gas flow rate.

In order to tune the specific input energy, the voltage applied is varied, but the frequency is kept constant: 50 Hz in the case of the adsorbed phase characterization setup and 200 Hz in the case of the gas phase monitoring setup. The gas flows are 750 mL/min and 200 mL/min respectively for the gas and solid phase setups, and the applied voltage is adapted to have comparable ozone productions. In all the measurements performed, electrical parameters are adjusted in order to keep the specific input energy around 5.3 J/L leading to a constant production of 22 ± 2 ppm.

2.3. Infrared diagnostics

Two complementary infrared techniques are used: gas phase measurements using Fourier Transform Infrared Spectroscopy (FTIR) and adsorbed phase measurements using Diffuse Reflectance Infrared Fourier Transform Spectroscopy (DRIFTS). Using the FTIR and DRIFTS cell in a complementary manner enables the thorough

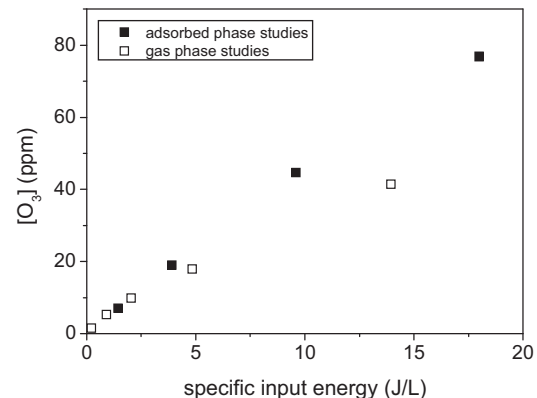


Fig. 2. Evolution of ozone produced by plasma setups as a function of specific input energy: (■) setup for characterization of the adsorbed phase, carrier gas is 20% O_2 balanced in Argon; (□) setup for characterization of the gas phase, carrier gas is 20% O_2 balanced in nitrogen.

Table 1
Assignment of vibrational wavenumbers for species of interest.

Vibration mode	Wavenumber (cm ⁻¹)	Wavenumber literature (cm ⁻¹) [31]
<i>Isopropanol study</i>		
ν_{OH}	3440	3570–3200
ν_{CH_3}	2973, 2936, 2872	2970–2860
$\delta_{\text{s}} \text{CH}_3$	1386	1380–1370
$\delta_{\text{as}} \text{CH}_3$	1465	1470–1430
$\delta_{\text{C}=\text{C}}$	1168	1300–700
$\delta_{\text{C}=\text{O}}$	1131	1050–1200
δ_{OH}	1293, 1252	1260–1350
$\delta_{\text{H}_2\text{O}}$	1640	1640
$\delta_{\text{as COO}}$	1553	1610–1550
$\nu_{\text{C}=\text{O}}$	1696	1690–1705
<i>Acetone study</i>		
ν_{OH}	3369	3570–3200
$\nu_{\text{CH}_3}, n_{\text{CH}}$	2971, 2936, 2919, 2865	2970–2860
δ_{CH_3}	1365, 1422, 1450	1470–1430
$\delta_{\text{C}=\text{C}}$	1238	1300–700
$\nu_{\text{C}=\text{O}}$	1696, 1667, 1734	1690–1725
$\nu_{\text{C}=\text{C}}$	1601	1600

analysis of reaction intermediates and species in both the gas and the adsorbed phase.

2.3.1. Gas phase analysis

The real time detection and quantification of the gas phase species (Fig. 1a) is performed using high resolution Nicolet 6700 Fourier Transform Infrared spectrometer (FTIR) equipped with a 10 m optical-path White cell and a cooled MCT (mercury cadmium telluride) detector. The cell is heated at 50 °C to ensure a good regulation and to prevent adsorption onto the mirrors. Two spectra per minute are collected with Omnic software with 16 scans per spectrum and a spectral resolution of 0.5 cm⁻¹. Detection limits of this analytical tool have been determined as two times the signal/noise ratio in the region of interest and are: 80 ppb for acetone, 90 ppb for IPA, 20 ppb for CO₂, 10 ppb for CO and 15 ppb for O₃. The assignments of vibrational bands for species of interest are reported in Table 1.

Calibration curves of organic species, CO₂ and CO are evaluated by passing 1.5 L min⁻¹ of standard gases in air at different concentrations through the FTIR gas cell. Ozone calibration is done using a 58 cm UV cell placed downstream the reactor. A deuterium lamp (Micropack DH2000) and a spectrometer (Ocean Optics USB4000) are used to measure the absorption of ozone at 254 nm.

2.3.2. Adsorbed phase analysis

In the adsorbed phase investigation apparatus, the adsorbent bed is located inside the DRIFTS cell, placed downstream the plasma reactor (Fig. 1b). This device allows a real time monitoring of the phenomena taking place on the material surface.

Diffuse Reflectance Infrared Fourier Transform Spectroscopy (DRIFTS) is also performed using a Nicolet 6700 Fourier Transform spectrometer applied for the *in situ* analysis of the adsorbent surface under a reactive atmosphere. This technique is extremely useful for non-transparent materials and allows the real time study of surface species coverage and product formation with a simultaneous measure of the reaction rates [32,33].

In the DRIFTS cell, the infrared beam is focused and sent on the material surface. Radiations diffused by the solid sample is collected by mirrors and sent to the detector [33]. The sample holder is a 15 mm long ceramic crucible with an internal diameter of 3.18 mm. The cell contains a heating resistor that can heat the sample up to 800 °C and the temperature is directly measured by a thermocouple in contact with the powder. Two spectra per minute are collected with Omnic software with 16 scans per spectrum and a spectral resolution of 4 cm⁻¹.

The main drawback of this technique is the difficulties related to quantitative measurements. No linear relation between band intensity and concentration of adsorbed species can be made [33,34]. Nevertheless, some recent works show the possibility of semi quantitative analysis with DRIFT spectroscopy [34,35]. Another limitation concerns the repeatability of the measurements. Since the diffusion coefficient varies with each preparation, it is difficult to compare the peak intensities of two spectra made with the same kind of material, but recorded during two different experiments [33].

However, it is possible to monitor the species evolution on the surface species using normalized values of peak intensities. The temporal evolution of the surface coverage (θ) of a species can be determined. The parameter θ is calculated by the ratio of the area of the corresponding peak over the maximal area obtained when saturation level is reached, thus, θ ranges from 0 to 1. The characteristic wavenumbers used for species identification are shown in Table 1.

2.4. Experimental procedure

The experimental procedure used for both experimental setups consists of five key steps:

- (i) *Pretreatment* of the TiO₂ sample at 300 °C to remove water and other adsorbed hydrocarbon species to guarantee surface repeatability.
- (ii) *Adsorption* of the pollutant on TiO₂ surface: the gas flow containing the pollutant passes through the sorbent bed and is gradually concentrated on the surface until saturation of the sorption sites.
- (iii) *Flushing with synthetic dry air flow* to remove reversibly adsorbed species. Flushing the adsorbent bed with pure air desorbs the molecules with the weakest heats of adsorption, i.e. physisorbed species, leaving only the irreversibly adsorbed molecules on the catalyst surface.
- (iv) *Surface exposition to ozone* by switching on the non-thermal plasma. Ozone generated by the plasma oxidizes the adsorbed molecules. The plasma is turned off after 70 min and the system is purged under dry synthetic air flow for a few minutes.
- (v) *Temperature programmed oxidation* under air flow at 300 °C is performed in order to oxidize the remaining adsorbed species and to regenerate the surface and complete the carbon balance.

Breakthrough curves are established during steps (ii) and (iii) and the quantities adsorbed are calculated by subtracting the area under the breakthrough curve to the area under the mixing curve. The mixing curve of the system is determined by by-passing the TiO₂ bed, in order to avoid the adsorption step. The quantities obtained in steps (iv) and (v) of the gas phase study are calculated by integrating the areas under the respective curve where the difference between the breakthrough and the mixing curve enables the calculation of the total amount of IPA and acetone adsorbed on TiO₂. Considering the different volumes of the reaction chambers, DRIFTS cell and gas phase reactor, the gas flow is adjusted in order to obtain a residence time in the sorbent vicinity of approximately 20 ms in both setups.

3. Results and discussion

3.1. FTIR gas phase study of IPA adsorption and oxidation by ozone

3.1.1. IPA adsorption: gas phase approach

Using the gas phase characterization setup, 98 ppm of IPA diluted in dry air is sent with a flow rate of 750 mL/min until

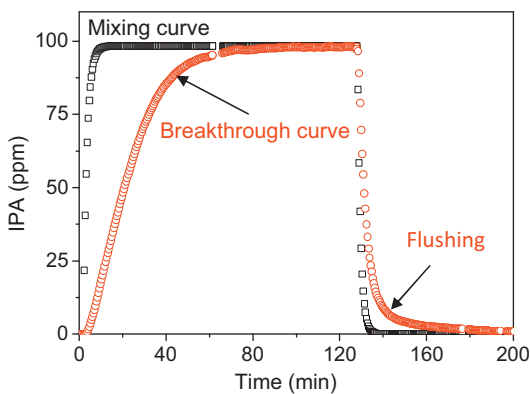


Fig. 3. IPA breakthrough curve and flushing curve monitored on TiO_2 surface under 750 mL/min in dry synthetic air at 295 K using the gas phase characterization setup.

130 min (breakthrough). Beyond 130 min only synthetic dry air is sent into the setup (flushing). The IPA breakthrough/flushing curve obtained is reported in Fig. 3. The rising part of the curve ($t < 130$ min) corresponds to the adsorption of IPA on the catalyst. The decay part of the curve ($t > 130$ min) corresponds to desorption of the weakly bonded IPA on the surface. The difference noticed between the flushing curve of IPA and the mixing curve allows the determination of the reversibly adsorbed fraction of IPA on TiO_2 , i.e. weakly bonded species. From a quantitative point of view, the amount of IPA initially adsorbed on TiO_2 has been determined as $6.9 \mu\text{mol}/\text{m}^2$. The flushing step leads to the desorption of $1.6 \mu\text{mol}/\text{m}^2$ of IPA which was reversibly adsorbed. The subtraction of these two values gives the amount of IPA irreversibly adsorbed on TiO_2 : $5.3 \pm 0.6 \mu\text{mol}/\text{m}^2$. This value is consistent with other values from the literature. Indeed, Sivachandiran et al. [27] reported a value of $7.6 \mu\text{mol}/\text{m}^2$ on P25-Degussa TiO_2 , and Larson et al. [25] a value of $6.9 \mu\text{mol}/\text{m}^2$. Lower values, ranging from 2 to $3 \mu\text{mol}/\text{m}^2$, were reported by El-Maazawi et al. [36], Rossi et al. [37] and Arsac et al. [23], but they were determined using PC500 Millenium TiO_2 .

3.1.2. Adsorbed IPA oxidation by O_3 : gas phase approach

After the flushing step, the TiO_2 surface is only covered by irreversibly adsorbed IPA. This surface is exposed to 20 ppm of O_3 generated by the plasma stage during 70 min (applied voltage 10 kV, frequency 50 Hz, injected power 68.2 mW, specific energy 5.5 J/L). Fig. 4a shows the temporal evolution of O_3 at the sorbent reactor outlet under three different conditions: (i) without TiO_2 in the reactor, (ii) with 200 mg of clean TiO_2 in the reactor, and (iii) with 200 mg of IPA saturated TiO_2 in the reactor.

As long as the sorbent reactor remains empty, ozone produced by the upstream plasma reaches the FTIR cell within a few minutes. When TiO_2 is introduced in the sorbent reactor, a significant difference is observed on the O_3 breakthrough curves; even after 70-min plasma, O_3 outlet concentration does not reach the input value. This behavior indicates that O_3 may be consumed on TiO_2 surface. According to Bulanin et al. [38], there are three main modes for ozone adsorption on TiO_2 : (i) weakly bonded molecules that form hydrogen bonds with OH groups and are physically adsorbed on the surface, (ii) molecules adsorbed on the weaker Lewis acid sites and (iii) interaction of ozone with strong Lewis acid sites. Only ozone adsorption on strong Lewis sites leads to the dissociation of the molecule to give a free O_2 molecule and a surface oxygen atom which remains attached to the titanium ion [38]. The presence of TiO_2 in the sorbent reactor induces the decomposition of a fraction of O_3 . The continuous increase of O_3 concentration at the outlet of the sorbent reactor indicates that the decomposition efficiency of O_3 on clean TiO_2 decreases with time. This behavior is consistent

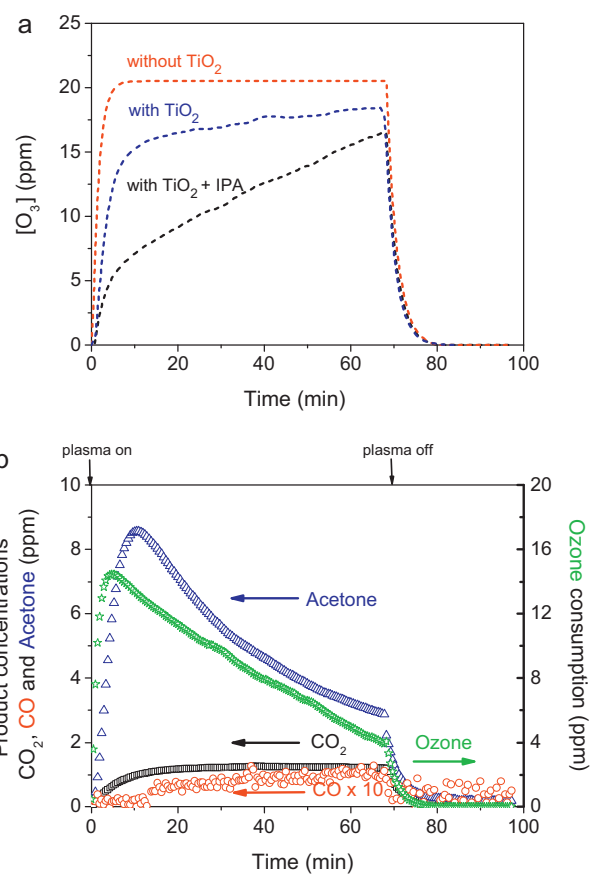


Fig. 4. (a) Temporal evolution of O_3 at the sorbent reactor outlet under three different conditions for the sorbent reactor. Ozone is produced by the upstream discharge (50 Hz, 10 kV, 68.2 mW, 5.5 J/L) using the gas phase characterization setup. (b) Gas phase product evolution (CO_2 , CO , acetone) at reactor output and ozone consumption during ozonation of IPA saturated TiO_2 surface (50 Hz, 10 kV, 68.2 mW, 5.5 J/L).

with an increasing coverage of strong Lewis acid sites, making them less and less available for further ozone adsorption.

As reported in Fig. 4a, when TiO_2 surface has been formerly saturated by irreversibly adsorbed IPA, the consumption of ozone is enhanced. This suggests that ozone is simultaneously consumed by TiO_2 Lewis acid sites and by adsorbed IPA. Thus IPA is expected to produce oxidized by-products when exposed to ozone. The difference between ozone consumption on clean TiO_2 and ozone consumption on IPA saturated TiO_2 corresponds to a quantity of ozone of $1.3 \mu\text{mol}/\text{m}^2$. So far we suggest that this amount reacts with adsorbed IPA, which leads to a ratio of 1 molecule of O_3 consumed for 4.5 molecules of IPA adsorbed on TiO_2 . From an energetic point of view, $0.046 \mu\text{mol}$ of ozone is consumed per injected joule of energy in the plasma. The temporal evolution of O_3 consumption during the plasma ON phase can be estimated from the difference between the curves with TiO_2 and with TiO_2 and IPA in Fig. 4a. This temporal evolution is compared with the IPA oxidation products: acetone, CO and CO_2 , presented in Fig. 4b.

Fig. 4b displays the evolution of the gas phase species detected during the exposition of IPA saturated TiO_2 surface to the 20 ppm ozone flow. IPA oxidation product concentrations are reported on the left axis. Ozone consumed as a consequence of the IPA adsorbed on the TiO_2 surface is reported on the right axis. The complete oxidation into CO and CO_2 remains relatively weak and a strong desorption of intermediate byproducts is observed with the acetone desorption. The mineralization of IPA into CO and CO_2 is first discussed.

3.1.3. IPA mineralization: gas phase approach

As the plasma is turned on, CO_2 production is directly noticed and O_3 starts to be consumed. CO_2 concentration reaches a plateau (ca. 1.2 ppm) within 20 min. Then, its production remains constant until the plasma is switched off. Around 12 min after plasma ignition, CO is latently observed with a concentration that slowly increases with time until plasma is turned off. We can consider that CO is produced since the beginning of the plasma ignition, but the concentrations evolved remains below the FTIR detection limits during the first 12 min. CO is produced as long as O_3 is sent on IPA covered TiO_2 ; nevertheless the level of CO hardly exceeds 80 ppb, which is 15 times lower than CO_2 . The production of CO_2 and CO , along with the immediate O_3 consumption of adsorbed IPA confirms that O_3 is able to oxidize, as well as mineralize, IPA adsorbed on TiO_2 . Subsequently, IPA oxidation can be first evaluated through the mineralization of the adsorbed organic matter into CO_2 and CO (Eq. (1)).

$$\text{Mineralization (\%)} = \frac{\text{QCO}_2 \pm \text{QCO}}{3 \times \text{QIPA}_{\text{irr}}} \times 100 \quad (1)$$

This mineralization rate, expressed in %, is calculated as the ratio of the total amount of carbon, QCO_2 and QCO , resulting from the oxidation of IPA into CO_2 and CO , respectively, over the carbon quantity of the pollutant initially adsorbed on the surface QIPA_{irr} . The amounts of CO and CO_2 produced are obtained from the integration of their temporal profiles in Fig. 4b. They can be expressed as a function of TiO_2 specific surface area. During the exposition of IPA saturated TiO_2 surface to plasma generated O_3 , the amount of CO_2 produced is $0.27 \mu\text{mol}/\text{m}^2$ and the amount of CO produced is $0.016 \mu\text{mol}/\text{m}^2$. These values could also be expressed per Joule of injected power leading to $8.5 \text{ nmol}/\text{J}$ and $0.5 \text{ nmol}/\text{J}$ for CO_2 and CO , respectively. Substituting the produced quantities of CO_2 and CO in $\mu\text{mol}/\text{m}^2$ into equation 1 gives a mineralization rate of only 2%.

As mentioned before, 0.2 O_3 molecule is consumed per IPA molecule adsorbed but 7 O_3 molecules are required to release 1 CO or CO_2 in the gas phase. Among the ozone reacting, most of the ozone is then used for producing other byproducts only partially oxidized. The strong release of acetone observed corresponds to this production of organic intermediates.

3.1.4. Formation of organic intermediates: gas phase approach

As soon as the discharge is turned on, a transient production of acetone with a maximum at 10 min is observed. The total amount of gas phase acetone produced within 70 min is $1.2 \mu\text{mol}/\text{m}^2$. Acetone is known to be an intermediate in IPA oxidation into CO_2 and CO . Upon the photocatalytic oxidation of IPA on TiO_2 , Larson et al. [25], Xu et al. [26] and Arsac et al. [23] have also observed a transient gas phase acetone production as a main intermediate during the oxidation of IPA. The amount of acetone detected in the gas phase is high since it corresponds to more than 22% of the irreversibly adsorbed IPA.

It is worth noting that ozone consumption also exhibits a maximum and then follows the same characteristic decay time as acetone (Fig. 4b). Thus, O_3 consumption seems to be related to acetone production. Maximum O_3 consumption occurs around 5 min, significantly before the maximum of acetone in the gas phase. This means that a first step involving O_3 must occur before acetone desorption. We can make the hypotheses that O_3 is first responsible for acetone production onto the surface and then desorption of acetone is triggered by another mechanism.

In order to understand this burst of acetone in the gas phase, the competitive adsorption of IPA vs. acetone on TiO_2 is studied using the gas phase characterization setup. The TiO_2 surface is initially saturated using 175 ppm of acetone diluted in air; subsequently, 98 ppm of IPA is sent onto the acetone saturated TiO_2 surface. The initial quantity of acetone adsorbed is determined as $3.7 \mu\text{mol}/\text{m}^2$.

The subsequent adsorption of IPA results in desorbing the totality of the acetone initially adsorbed on TiO_2 , and the obtained amount of irreversibly adsorbed IPA is $6.3 \mu\text{mol}/\text{m}^2$. Second, the reverse experiment is done with an initial IPA adsorption followed by a subsequent acetone adsorption. The quantity of IPA irreversibly adsorbed is $6.1 \mu\text{mol}/\text{m}^2$. When acetone is consequently sent, only $0.4 \mu\text{mol}/\text{m}^2$ of acetone is irreversibly adsorbed on the surface and results in the desorption of $0.4 \mu\text{mol}/\text{m}^2$ of IPA.

This confirms that a competitive adsorption occurs between IPA and acetone to access similar adsorption sites on TiO_2 . When TiO_2 surface is fully saturated with IPA, only a small fraction of surface sites are accessible for irreversible adsorption of acetone. An experimental study of competitive adsorption between IPA and acetone has been conducted by Arsac et al. [23], the authors show that IPA adsorbed species may be photocatalytically oxidized into acetone and then CO_2 . Similarly to our experiments, acetone is transiently produced. Arsac et al. [23] evidenced that an acetone molecule formed by the photocatalytic oxidation of IPA adsorbed on a "S₁" site cannot remain adsorbed on the TiO_2 surface: it must either desorb rapidly as gaseous acetone or diffuse on the surface to be adsorbed on "S₂" sites, specific to acetone, or on the "S₁" sites liberated by the removal of IPA surface species during oxidation [23]. As a consequence, the transient gas phase production of acetone observed in Fig. 4b can be explained by (i) the oxidation of IPA into acetone in the adsorbed phase, and (ii) the competitive adsorption between the two species on TiO_2 sites leading to the release of acetone in the gas phase when IPA surface coverage is still high.

Apart from acetone, no other organic species is observed in the gas phase by FTIR while the plasma is switched on. Taking into account gas phase acetone, CO and CO_2 , 24% of the irreversibly adsorbed IPA has been converted into a species monitored in the gas phase at the reactor output. When the plasma is switched off, the concentrations of all the species depicted in Fig. 4b gradually drop to zero. The decay time observed corresponds well to that required for purging the cell, which confirms that the observed products are oxidation products under ozone flow.

To complete the gas phase study and to elucidate the observed phenomena, surface species have been monitored during steps (ii)–(iv) of the experimental procedure.

3.2. *In situ* DRIFTS study of IPA adsorption and oxidation by ozone

3.2.1. Adsorption of IPA: adsorbed phase approach

After pretreatment of the TiO_2 surface, 160 ppm of IPA diluted in 20% O_2 /Ar is sent into the experimental setup dedicated to the adsorbed phase characterization (Fig. 1a), with a total flow rate of 200 mL/min. DRIFT spectra are recorded in the range 1000 – 3600 cm^{-1} during the breakthrough of IPA on TiO_2 inserted into the analytical device. The DRIFT spectrum of clean TiO_2 surface recorded under dry air atmosphere after the 300°C pretreatment is subtracted to the spectra collected during the adsorption. The obtained spectra are shown in Fig. 5.

It clearly appears in Fig. 5 that the introduction of IPA in the system leads to the appearance of several new absorption bands located at 3440 (broad), 2973 , 2936 , 2872 , 1640 , 1465 , 1386 , 1293 , 1252 , 1168 and 1131 cm^{-1} . In the lower wavenumber range, three main bands indicate the dissociative adsorption of IPA onto TiO_2 . The bands at 1386 cm^{-1} ($\delta_{\text{S-CH}_3}$) and at 1168 cm^{-1} ($\delta_{\text{C-C}}$) can be ascribed to isopropoxide species, indicating a first adsorption mode of IPA which seems to be dissociative. In addition, the band at 1131 cm^{-1} ($\delta_{\text{C-O}}$) indicates the formation of isopropoxy groups confirming a dissociative adsorption of IPA [23,25,26,37]. The production of OH groups resulting from IPA dissociative adsorption can be noticed on the high wavenumber range. Indeed, a large band with a maximum at 3440 cm^{-1} corresponding to the OH stretch (ν_{OH}) of interacting hydroxyl groups increases with

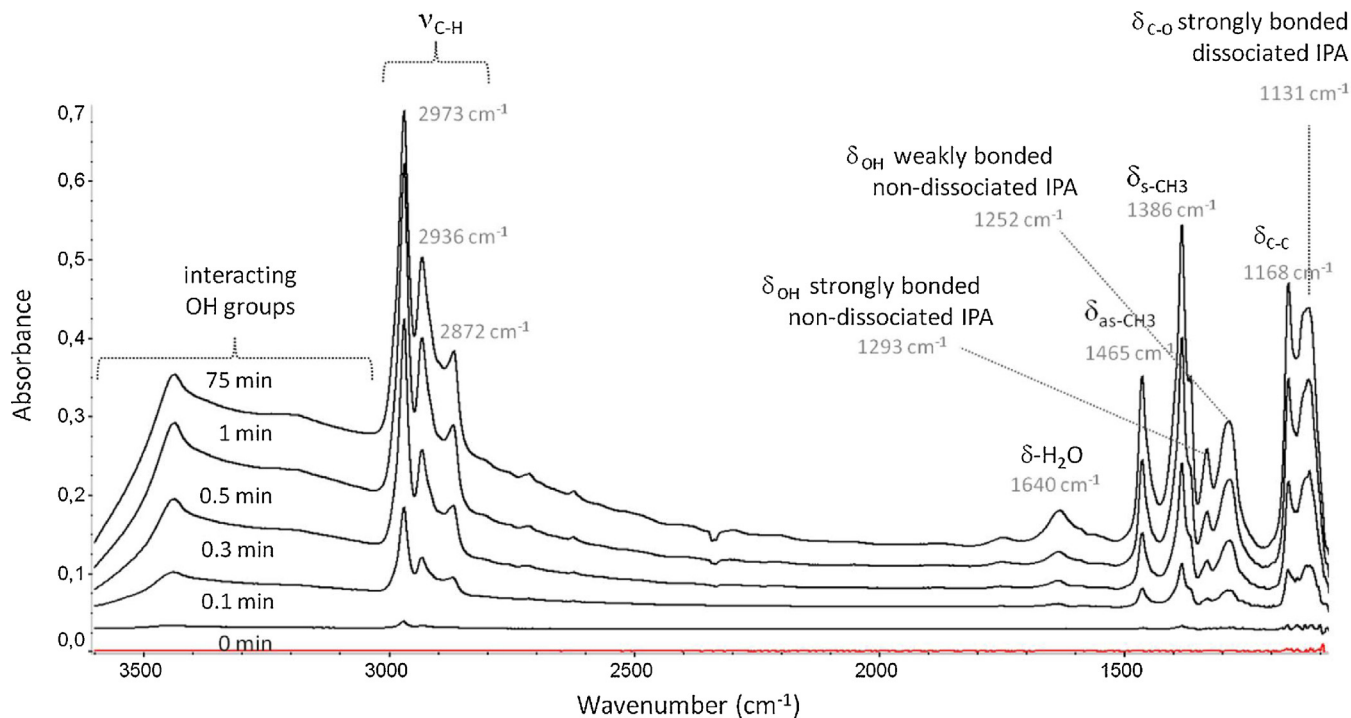


Fig. 5. DRIFTS absorbance spectra recorded during IPA adsorption on TiO_2 at 295 K under 200 mL/min of 20%O₂/Ar.

IPA breakthrough on TiO_2 surface. This is consistent with the increase of the band at 1640 cm^{-1} ($\delta_{\text{H}_2\text{O}}$) ascribed to molecular H_2O physisorbed on TiO_2 surface, also resulting from the dissociative adsorption of IPA [39].

Another, non dissociative, adsorption mode of IPA can also be evidenced on the spectra of Fig. 5. The band recorded at 1293 cm^{-1} (δ_{OH}) along with the previously mentioned bands at 3440 cm^{-1} (ν_{OH}) are ascribed to the hydroxyl of strongly bonded un-dissociated IPA species on Ti(IV) Lewis acid sites [23,25,26,37]. More generally, the bands appearing at 2973 , 2936 and 2872 cm^{-1} correspond to methyl (ν_{CH_3}) symmetric and asymmetric stretch modes of adsorbed IPA species [23,25,26,37]. These bands are accompanied by the methyl C–H bands ($\delta_{\text{s-CH}_3}$) at 1386 cm^{-1} and ($\delta_{\text{as-CH}_3}$) at 1465 cm^{-1} . A second non-dissociative adsorption mode could be identified through an additional (δ_{OH}) band at 1252 cm^{-1} , of a weakly hydrogen-bonded IPA species. This mode is also proposed by Arsac et al. [24], Rossi et al. [37] and Larson et al. [25].

In summary, the results have shown that the adsorption of IPA on TiO_2 is done via two main adsorption modes, a dissociative one and a non-dissociative one [23,25,37], represented in Fig. 6.

- (i) The dissociative adsorption results in the formation of monodentate isopropoxy groups and surface hydroxyl species.
- (ii) The non-dissociative adsorption gives rise to strongly bonded isopropanol coordinated to surface Lewis acid sites and weakly hydrogen-bonded isopropanol to surface basic sites.

The two main adsorption modes can only be distinguished by the δ_{OH} and $\delta_{\text{C-O}}$ vibrations. The other vibrations provide absorption bands strongly overlapped such as $\nu_{\text{as-CH}_3}$ at 2973 cm^{-1} and $\nu_{\text{s-CH}_3}$ at 2936 cm^{-1} . It is interesting to note that when the gas flow was switched back to pure O₂/Ar, a small decrease was noticed in the intensities of all the IPA peaks. This can be attributed to the desorption of the weakly bonded species of both forms of IPA, dissociated and non-dissociated. This is consistent with our observations made on the desorption of $1.6\text{ }\mu\text{mol/m}^2$ of weakly adsorbed IPA species using the gas phase monitoring setup.

3.2.2. Adsorbed IPA oxidation by O₃: adsorbed phase approach

After the adsorption/flushing step discussed in the previous section, the discharge is turned on in order to generate O₃ upstream the sorbent reactor (applied voltage 2.5 kV, frequency 200 Hz, injected power 11.7 mW, specific energy 4.7 J/L, ozone concentration 23 ppm). The evolution of the adsorbed species monitored by DRIFTS during the ozonation of the surface is shown in Fig. 7.

On the spectrum corresponding to $t=0$, the IPA peak at 2973 cm^{-1} attributed to IPA is at its highest and no carbonyl vibration ($\nu_{\text{C=O}}$) is detected. This indicates that no acetone can be detected as long as the plasma is turned off. Once the plasma is turned on, all the bands corresponding to IPA adsorption modes decrease and new bands appear at 1696 cm^{-1} and 1553 cm^{-1} . The band at 1696 cm^{-1} is characteristic of the ($\nu_{\text{C=O}}$) vibration mode of the carbonyl group in acetone and the band at 1553 cm^{-1} is characteristic of the ($\delta_{\text{as-COO}}$) vibration mode of formate species [23,26]. After 20 min of plasma, a band at 1701 cm^{-1} appears on the IR spectrum. This band is ascribed to ($\nu_{\text{C=O}}$) of an aldehyde species (acetaldehyde or formaldehyde) [39]. The temporal evolution of the peaks characteristic of both adsorption modes of IPA can be followed by plotting the TiO_2 surface coverage of dissociated IPA ($\delta_{\text{OH}} = 1252\text{ cm}^{-1}$) and non-dissociated IPA ($\delta_{\text{C-O}} = 1131\text{ cm}^{-1}$) as a function of time. The obtained data is plotted in Fig. 8.

It clearly appears in Fig. 8 that the temporal decays of both IPA adsorption modes during ozonation are the same. This means that, independently of the adsorption mode, dissociated and non-dissociated IPA on TiO_2 show the same reactivity with ozone. Simple models described in the literature suggest that O₃ decomposes on TiO_2 surface, leading to O₂ in the gas phase and an adsorbed O atom [26,38]. This species is considered as the main oxidizing species and a Langmuir–Hinshelwood kinetic model is proposed to describe the reaction between the adsorbed VOC and the adsorbed O atoms. Since the binding energy and the chemical nature of the bonds differ between the dissociated and non-dissociated IPA, a difference should be observed in the temporal decays because the reaction rates should be different between O atoms and the two different IPA adsorbed modes. Thus, we suggest

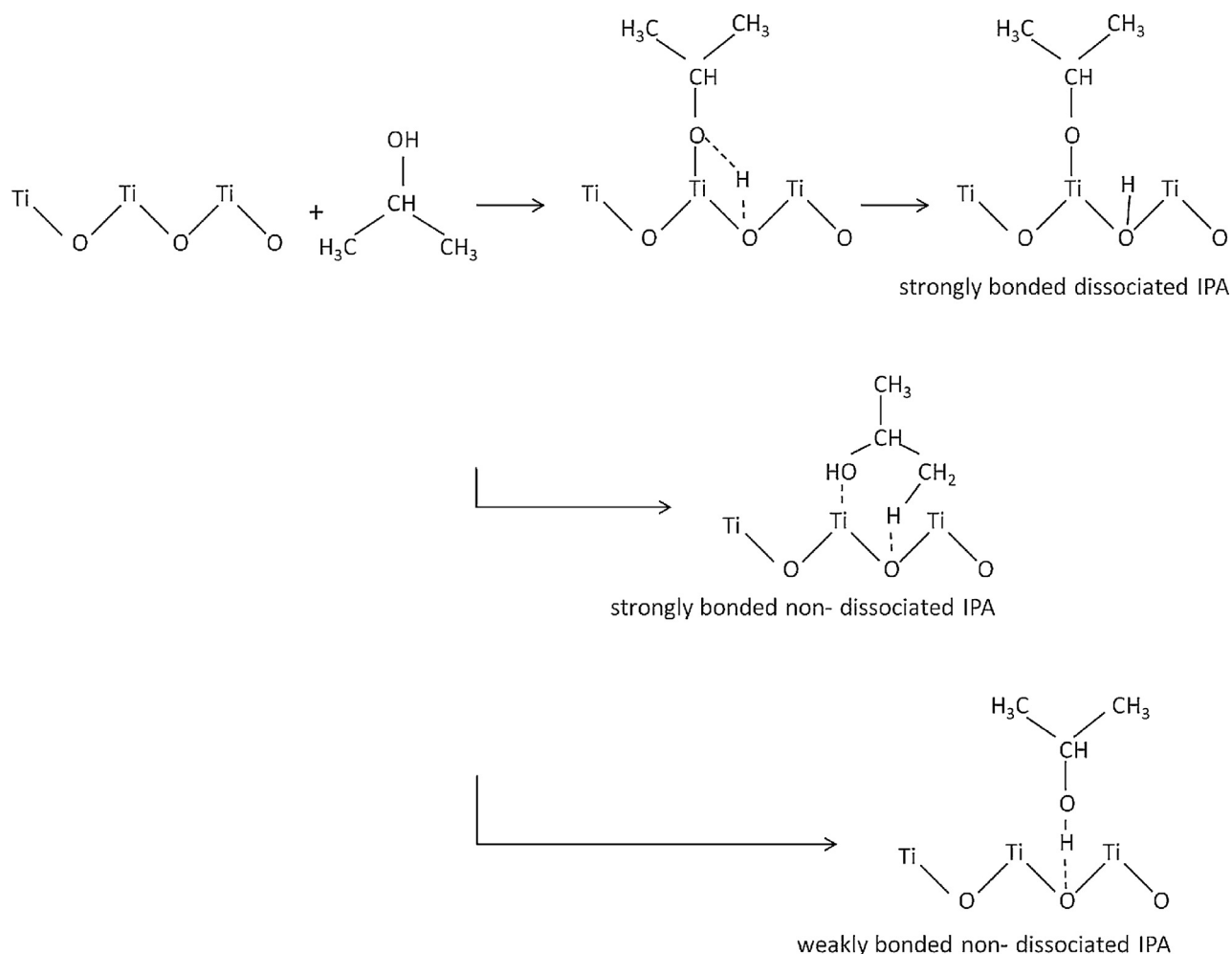


Fig. 6. Schematic representation of IPA adsorption modes on TiO_2 .

that O atoms may not be the main oxidizing species and O_3 or surface hydroxyl groups could directly take part in the oxidation reactions. Another kinetic model should be applied to describe the process, further investigations are required. Considering the same reactivity of both species, the peak at 2973 cm^{-1} , common to both species, is used to follow the temporal evolution of IPA in Fig. 9.

So far, it can be noted that IPA oxidation proceeds via acetone in both investigated oxidation methods. Acetone seems to be the main intermediate and single route of IPA oxidation to yield CO_2 and water on TiO_2 [23,24]. Moreover, it was shown that acetone and formate species accumulate on the TiO_2 surface during the ozonation step and that the mineralization of IPA is not complete. It can

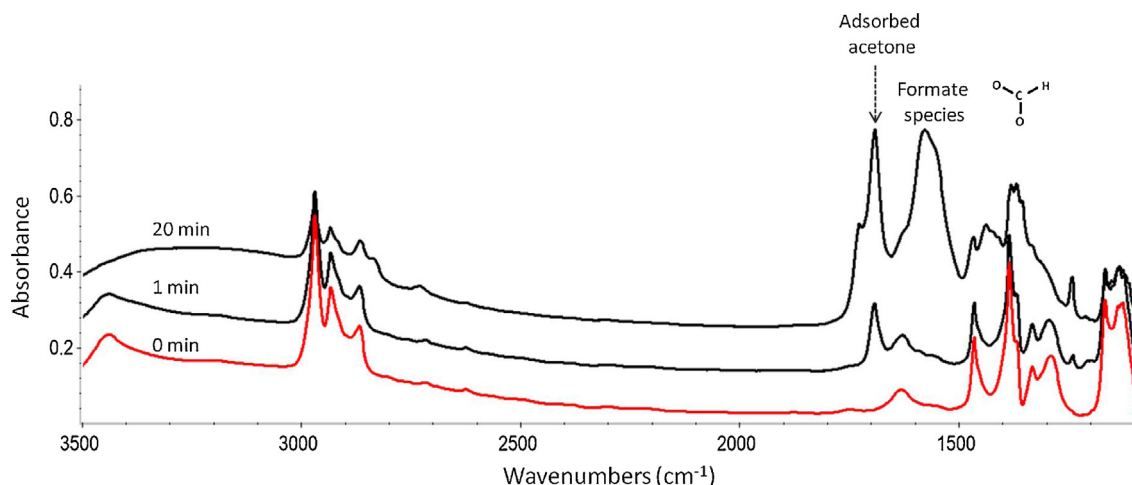


Fig. 7. Evolution of surface species adsorbed on TiO_2 during ozone generation under 200 mL/min of $20\% \text{ O}_2/\text{Ar}$ (200 Hz, 2 kV, 11.7 mW, 4.7 J/L).

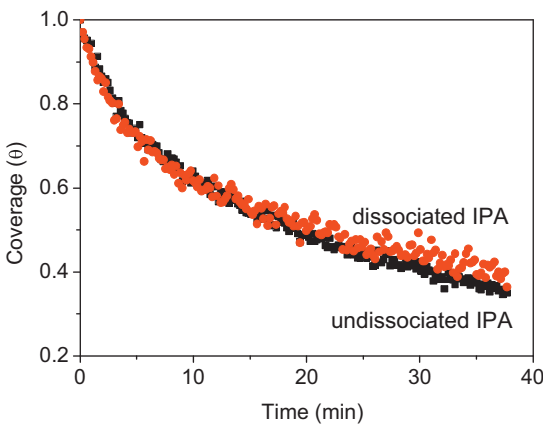


Fig. 8. Evolution of dissociated and non-dissociated IPA surface coverages on TiO_2 during the ozonation phase under 200 mL/min of 20% O_2/Ar and 23 ppm of O_3 (DRIFTS).

be assumed that if the surface is saturated with IPA beforehand, the plasma will not lead to a complete mineralization.

3.2.3. Formation of intermediates: adsorbed phase approach

The evolutions of IPA, acetone and formate species adsorbed on TiO_2 as a function of ozonation time are reported in Fig. 9. At $t=0$, the surface is saturated with IPA, thus, $\theta_{\text{IPA}}=1$ and $\theta_{\text{acetone}}=0$. IPA surface coverage decreases as a function of time and acetone coverage gradually increases until it reaches a plateau at approximately 20 min. In parallel to the formation of acetone, the formation of formate species (HCOO^-) can be noticed from the peak at 1553 cm^{-1} .

The competitive adsorption study between IPA and acetone reported in Section 3.1.4 emphasized the predominant adsorption of IPA on adsorption sites: ' S_1 ' sites. In the presence of IPA on TiO_2 surface, Arsac et al. [23] have evidenced that acetone may irreversibly adsorb on dedicated sites: ' S_2 ' sites. Even when IPA surface coverage decreases, the presence of adsorbed acetone is completely controlled by the strong competitive chemisorptions between IPA and acetone. Arsac et al. [23] evaluate that the amount of acetone which can be adsorbed onto ' S_2 ' sites remains lower than 10% of the total amount of TiO_2 sites able to adsorb irreversibly acetone. Based on the results reported in Section 3.1.4, we can estimate that a maximum of $0.4\text{ }\mu\text{mol}/\text{m}^2$ of acetone adsorbs on ' S_2 ' sites under our conditions. As reported in Fig. 9, the surface coverage of acetone becomes stable after 20 min, whereas IPA surface coverage still decreases. We can consider that within a 20 min ozonation period,

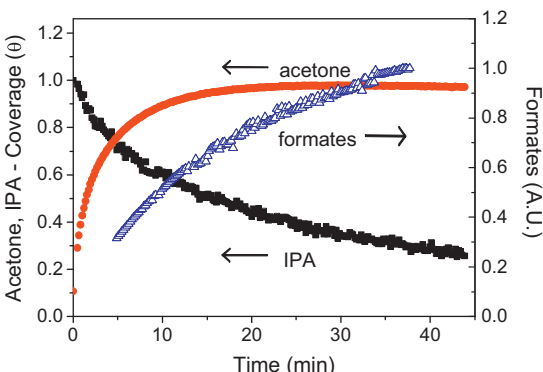


Fig. 9. Evolution of IPA, acetone and formates apparent surface coverages on TiO_2 during the ozonation phase under 200 mL/min of 20% O_2/Ar and 23 ppm of O_3 (DRIFTS). Since acetone oxidation has been evidenced as a key step in the oxidation, its adsorption on TiO_2 and reaction with O_3 is more specifically investigated in the following section.

the ' S_2 ' sites are saturated; equilibrium is reached regarding acetone adsorption on ' S_2 ' sites. As evidenced by the presence of CO and CO_2 in the gas phase and formates in the adsorbed phase, adsorbed acetone can be further oxidized. The further oxidation of acetone can make a ' S_2 ' adsorption site free. Acetone produced by IPA adsorbed on S_1 sites can: (i) either desorb to the gas phase, if no ' S_2 ' sites are available; or (ii) diffuse toward an available ' S_2 ' site.

Considering the proposed pathway, CO_2 may only be produced from the oxidation of ' S_2 ' adsorbed acetone. The constant formation of CO_2 during ozonation reported in the gas phase monitoring section is reached within 20 min (Fig. 4b) which corresponds to the typical time scale to saturate ' S_2 ' sites with adsorbed acetone (Fig. 9). This is also in accordance with the microkinetic approach developed by Arsac et al. [23] for IPA photocatalytic oxidation, that points out the oxidation of ' S_2 ' adsorbed acetone as the limiting step for CO_2 formation. Finally, considering that to be mineralized into CO_2 or CO , adsorbed IPA necessarily goes through ' S_2 ' adsorbed acetone, adsorbed formates can either be considered as reaction intermediates between ' S_2 ' adsorbed acetone and CO_2 , or as by-products, since no evidence of CO_2 formation from formates under ozonation has been found yet.

3.3. FTIR gas phase study of acetone adsorption and oxidation by ozone

3.3.1. Acetone adsorption: gas phase approach

Similarly to the previous IPA study, 175 ppm of acetone in air is sent to the TiO_2 sorbent bed with a total synthetic air flow of 750 mL/min. Once the inlet concentration of acetone is reached at the sorbent reactor outlet (breakthrough), the excess of acetone is flushed under pure synthetic air (flushing). Acetone breakthrough and flushing curves are compared with the corresponding system's mixing curves. The total quantity of initially adsorbed acetone is $5.3\text{ }\mu\text{mol}/\text{m}^2$. The reversibly adsorbed amount removed by the flushing step is $3.4\text{ }\mu\text{mol}/\text{m}^2$, giving $1.9 \pm 0.6\text{ }\mu\text{mol}/\text{m}^2$ of acetone irreversibly adsorbed on TiO_2 . The amount of irreversibly adsorbed acetone on clean TiO_2 surface is nearly 3 times lower than the amount of irreversibly adsorbed IPA. This point evidences that, even in the absence of IPA, the coverage of ' S_1 ' sites by acetone is poor, otherwise irreversibly adsorbed amount of acetone would have been higher. We therefore suggest that acetone preferentially adsorbs on ' S_2 ' sites during the single adsorption of acetone on TiO_2 .

3.3.2. Adsorbed acetone reaction with O_3 : gas phase approach

In a first step the consumption of O_3 by acetone adsorbed TiO_2 surface has been investigated. Ozone is produced during 70 min by switching on the discharge (applied voltage 10 kV, frequency 50 Hz, injected power 72 mW, specific energy 5.8 J/L, ozone concentration 24 ppm). Similarly to Section 3.1.2, the breakthrough of plasma generated ozone has been monitored by gas phase FTIR at the sorbent reactor outlet. Three different conditions are reported in Fig. 10 and compared:

- The sorbent reactor is empty: this curve enables the ozone mixing curve determination of the gas phase analysis setup.
- The sorbent reactor contains clean TiO_2 : similarly to Fig. 4a, $0.51\text{ }\mu\text{mol}/\text{m}^2$ of O_3 is consumed on TiO_2 surface.
- The sorbent reactor contains acetone saturated TiO_2 : an additional consumption of O_3 is evidenced as TiO_2 surface is saturated by acetone. This points out the possible reaction of O_3 with adsorbed acetone. The amount of ozone which has been consumed by adsorbed acetone can be estimated as $2.1\text{ }\mu\text{mol}/\text{m}^2$. This value is almost twice higher than the amount of ozone consumed by IPA saturated TiO_2 surface. It

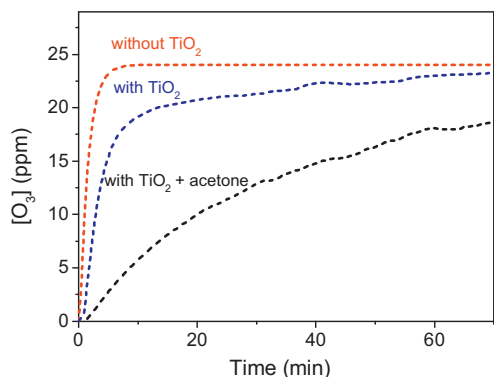


Fig. 10. Temporal evolution of O_3 at the sorbent reactor outlet under three different conditions for the sorbent reactor. Ozone is produced by the upstream discharge (50 Hz, 10 kV, 72 mW, 5.8 J/L) using the gas phase characterization setup.

corresponds to the consumption of 1.1 molecule of ozone for 1 molecule of adsorbed acetone.

The reaction of ozone with adsorbed acetone is confirmed by the presence of oxidation side-products in the gas phase at the sorbent reactor outlet. The difference between ozone consumption on clean TiO_2 and ozone consumption on IPA and acetone saturated TiO_2 taken from Figs. 4b and 10 is plotted in Fig. 11.

The oxidation of IPA results in a faster consumption of ozone on a short time scale (~ 5 min). This proves that adsorbed IPA is more easily oxidized by ozone than acetone. This can be due to the higher surface coverage of IPA compared to acetone and/or to a higher reactivity of IPA with ozone. On a longer time scale, ozone consumption is relatively the same for both experiments.

The oxidation products observed in the gas phase (Fig. 12) are CO_2 and CO , with $0.3 \mu\text{mol}/\text{m}^2$ and $0.04 \mu\text{mol}/\text{m}^2$, respectively. These values correspond to 8.9 and 1.2 nmol of CO_2 and CO produced per injected Joule, respectively. These values are very close to those determined during IPA ozonation (Section 3.1.3). This could be consistent with the fact that, to be mineralized, IPA has to be first converted into acetone and that acetone oxidation is the key step of the oxidation process. In the case of adsorbed acetone ozonation, CO_2 and CO productions follow the same trend with an initial peak that slowly and gradually decreases. In the case of adsorbed IPA ozonation, CO and CO_2 are constant along the 70-min ozonation period. In the case of acetone, the decrease of CO_2 and CO at the sorbent reactor outlet could be attributed to the depletion of adsorbed acetone. However, the CO_2 and CO amounts produced during the 70-min ozonation period only correspond to the mineralization of 6% of irreversibly adsorbed acetone. It suggests that

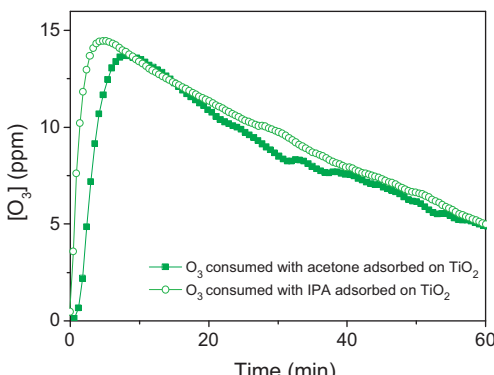


Fig. 11. Comparison of ozone consumption on IPA saturated TiO_2 (□) and acetone saturated TiO_2 (■).

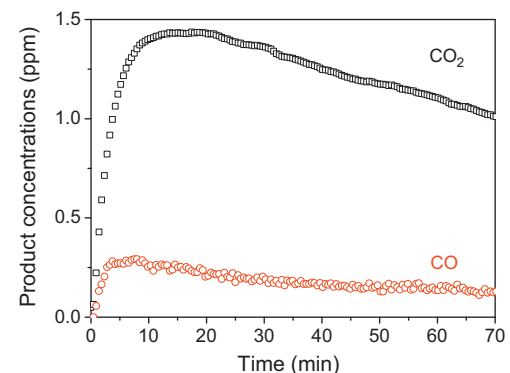


Fig. 12. Gas phase product evolution (CO_2 , CO) at reactor output and ozone consumption during ozonation of acetone saturated TiO_2 surface (50 Hz, 10 kV, 72 mW, 5.8 J/L).

organic reaction intermediates may be stored in large amounts on TiO_2 surface during ozonation. This point is investigated using the surface characterization setup in the following section.

3.3.3. Adsorption of acetone: adsorbed phase approach

After pretreatment of the TiO_2 surface, 640 ppm of acetone diluted in 20% O_2 /Ar is sent into the experimental setup dedicated to the adsorbed phase characterization (Fig. 1b), with a total flow rate of 200 mL/min. DRIFTS spectra are recorded in the range 1200 – 3600 cm^{-1} during the breakthrough of acetone on TiO_2 inserted into the analytical device. The DRIFTS spectrum of clean TiO_2 surface recorded under dry air atmosphere after the 300°C pretreatment is subtracted to the spectra collected during the adsorption. The obtained spectra are shown in Fig. 13. Adsorption of acetone on TiO_2 surface leads to the emergence of typical absorption bands at 3369 (broad), 2971 , 2936 , 2919 , 2865 , 1696 , 1667 , 1601 , 1450 , 1422 , 1365 and 1238 cm^{-1} . The adsorbed acetone species are characterized by the $\nu_{C=O}$ stretching vibration at 1696 cm^{-1} , the δ_{CH_3} at 1422 – 1365 cm^{-1} and the δ_{C-C} bending at 1238 cm^{-1} [20,36]. As the breakthrough of acetone is performed, the intensity of the bands attributed to acetone initially increases and then decreases. In parallel, other bands are continuously increasing on the spectra, they are located at 1667 , 1601 , and 1450 cm^{-1} and have been respectively ascribed to the $\nu_{C=O}$, ν_{C-C} and $\delta_{as} CH_3$ vibration modes of mesityl oxide [37,38]. The large band in the 3300 – 3400 cm^{-1} region correspond to interacting OH groups and the peaks between 2971 and 2865 cm^{-1} represent the asymmetric and symmetric stretch of methyl and methyne groups of the two organic compounds.

The formation of mesityl oxide on TiO_2 surface along with acetone adsorption has been formerly evidenced by Coronado et al. [40], El-Maazawi et al. [36], and Xu et al. [26]. The temporal evolutions of adsorbed acetone and mesityl oxide during acetone breakthrough on TiO_2 surface are plotted in Fig. 14. During the first 3 min, acetone surface coverage on TiO_2 increases steeply whereas mesityl oxide is not observed on the surface. As soon as the surface coverage of acetone reaches 0.35, the production of mesityl oxide starts. This behavior suggests that mesityl oxide formation is conditioned to an acetone surface coverage threshold. The same behavior is noticed by El-Maazawi et al. [36] using Langmuir adsorption technique. They report a threshold regarding acetone surface coverage of 0.3 which is consistent with our result. The sudden increase in acetone surface coverage temporal evolution at $t = 3$ min, corresponding to mesityl oxide initial production, indicates that acetone adsorption sites are released by mesityl oxide formation. Mesityl oxide originates from aldol condensation of two adsorbed acetone molecules; it corresponds to a dehydration reaction which leads to the release of a water molecule, which can be observed with

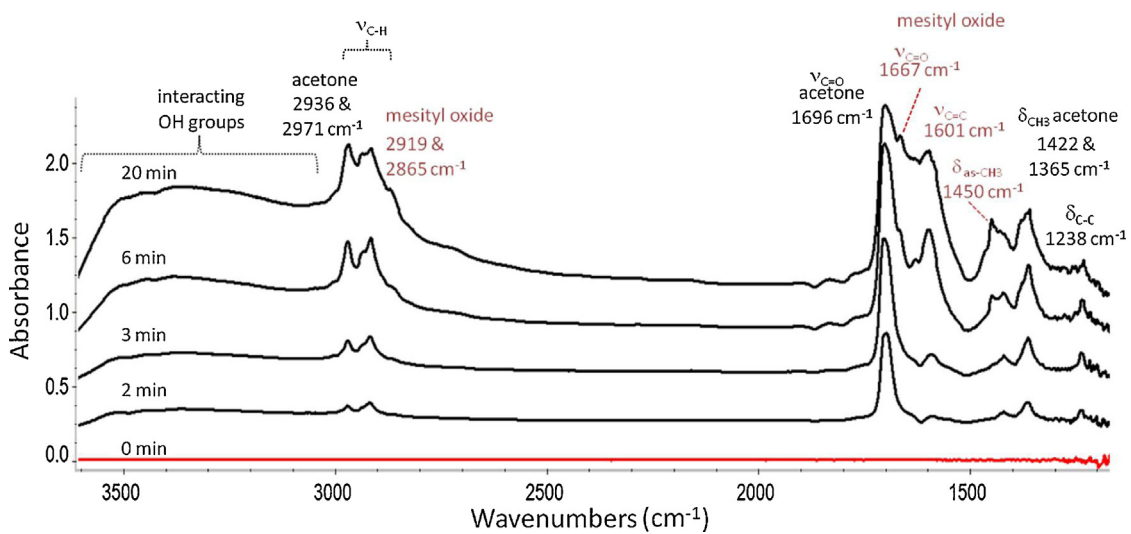


Fig. 13. DRIFTS absorbance spectra of recorded during acetone adsorption on TiO_2 at 295 K under 200 mL/min of 20%O₂/Ar.

the increasing peak in the 3300–3400 cm^{-1} region of the spectra in Fig. 13. Based on the determination of the partition between acetone and mesityl oxide as a function of acetone surface coverage proposed by El-Maazawi et al. [36], it is possible to estimate that almost 50% of the adsorbed acetone molecules are converted into mesityl oxide under our experimental conditions.

3.3.4. Ozonation of acetone saturated TiO_2 surface: adsorbed phase approach

As acetone saturated TiO_2 surface is submitted to plasma generated ozone exposure, acetone and mesityl oxide are present in the adsorbed phase. During this treatment, the temporal evolution of adsorbed acetone can be followed through the evolution of the band at 1696 cm^{-1} corresponding to $\nu_{\text{C=O}}$. Obtained data are reported in Fig. 15. The decrease in acetone surface coverage and the exposure of the surface to O₃ are simultaneous. In parallel, as soon as the discharge is switched on, the peak at 1601 cm^{-1} is broadened. During the adsorption step, this peak was attributed to adsorbed mesityl oxide; however, considering the oxidative treatment, it could also be attributed to adsorbed formate species formed on the surface. So far, the spectral resolution of the DRIFTS system does not make possible the distinction between adsorbed formates and mesityl oxide, and no clear trend is observed in the region 1550–1650 cm^{-1} . The apparition of a new peak at 1734 cm^{-1} is observed a few minutes

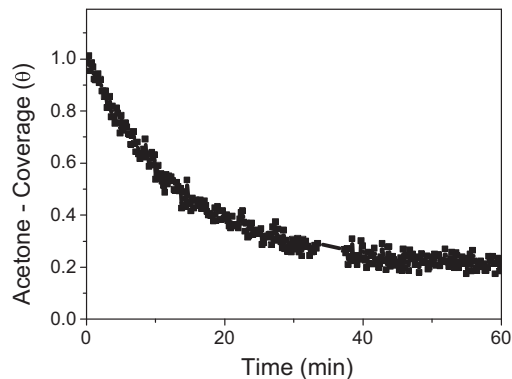


Fig. 15. Evolution of acetone surface coverage on TiO_2 during the ozonation phase under 200 mL/min of 20%O₂/Ar (DRIFTS).

after the plasma is switched on, it is attributed to the $\nu_{\text{C=O}}$ of formic acid [41]. Thus, it clearly appears that acetone is oxidized, but it is not possible to determine precisely the nature of the side products, apart from formic acid and formate species that remain adsorbed on the surface.

Acetone surface coverage and the evolution of formic acid are monitored and shown in Figs. 15 and 16, respectively. As the plasma is switched on, a direct oxidation of acetone takes place and its surface coverage decreases with time. The oxidation of the initially

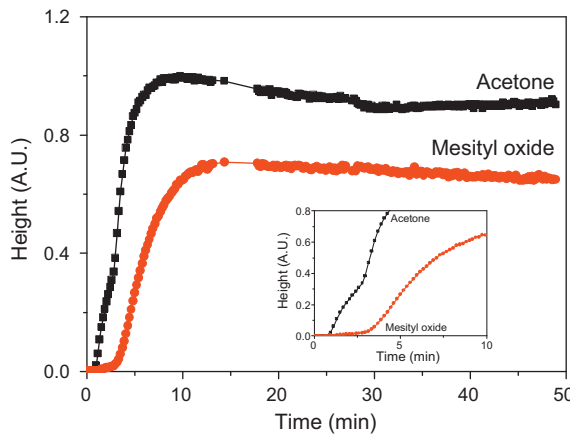


Fig. 14. Evolution of acetone and mesityl oxide apparent surface coverages on TiO_2 during the adsorption of acetone under 200 mL/min of 20%O₂/Ar (DRIFTS).

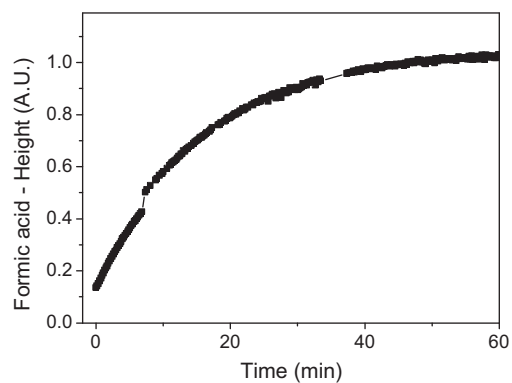


Fig. 16. Evolution of formic acid peak intensity on TiO_2 during the ozonation phase under 200 mL/min of 20%O₂/Ar (DRIFTS).

adsorbed species, acetone and mesityl oxide (not shown) by ozone leads to the formation of CO₂ and CO in the gas phase (Fig. 12) as well as formic acid (Fig. 16) and formates (not shown) that remain on the surface of TiO₂ in the present conditions. Other products could be formed but are not detectable in the given conditions. Gas phase CO₂ and CO do not follow the same trend as adsorbed formic acid. Formic acid increases with time whilst CO₂ and CO production decrease approximately 10 min. after the plasma is turned on (Fig. 12). The gas phase oxidation products probably result from the direct oxidation of acetone and mesityl oxide species. Even though the trend of formate accumulation on the surface is not followed, the formation of formic acid could be linked to that of formates, with the two species being in equilibrium on the TiO₂ surface.

4. Conclusion

The present study uses the simultaneous analysis of gas phase and surface species via FTIR and DRIFTS measurements to understand the mechanisms of IPA and acetone oxidation on TiO₂ exposed to ozone flow.

The adsorption of IPA onto TiO₂ leads to a dissociated and non-dissociated species, showing the same reactivity with respect to ozone. The ozonation of the saturated surface leads to CO₂, CO and a transient acetone production. A competitive adsorption occurs between IPA and acetone to access similar adsorption sites denoted "S₁" on TiO₂. When TiO₂ surface is fully saturated with IPA, only a small fraction of surface sites denoted "S₂" are accessible for irreversible adsorption of acetone and its subsequent oxidation into CO₂. As a consequence, acetone is released in the gas phase as an oxidation intermediate. This phenomenon is explained by (i) the oxidation of IPA into acetone in the adsorbed phase and (ii) the competitive adsorption between the two species on TiO₂ sites leading to the release of acetone in the gas phase when IPA surface coverage is still high.

The adsorption of acetone on TiO₂ also leads to mesityl oxide formation by aldol condensation. As ozonation takes place, gas phase CO₂ and CO are observed accompanied by formates and formic acid that remain adsorbed on the surface.

The non-thermal plasma oxidation of IPA yields 8.5 nmol of CO₂ per injected joule of energy and 8.9 nmol of CO₂ per injected joule in the case of acetone. The similar quantities of CO₂ produced show that oxidation into CO₂ is dependent on "S₂" sites for both studies and that the oxidation of IPA and acetone have the same limiting step.

Acknowledgements

This work has been partly supported by ANR Grant RAMPE (NT09_507899), Labex Plas@Par, AL-KO Therm and AL-KO SAS.

References

- [1] V. Nehra, A. Kumar, H.K. Dwivedi, *Int. J. Eng. 2* (2008) 53–68.
- [2] EU directive 2004/42/CE.
- [3] F. Holzer, U. Roland, F.-D. Kopinke, *Appl. Catal. B: Environ.* 38 (2002) 163–181.
- [4] H.-H. Kim, *Plasma Process. Polym.* 1 (2004) 91–110.
- [5] U. Kogelschatz, *Plasma Chem. Plasma Process.* 23 (2003) 1–46.
- [6] M. Magureanu, N.B. Mandache, P. Eloy, E.M. Gaigneaux, V.I. Parvulescu, *Appl. Catal. B: Environ.* 61 (2005) 12–20.
- [7] B. Penetrante, M.C. Hsiao, J.N. Bradbury, B.T. Merritt, G.E. Vogtlin, A. Kuthi, C.P. Burkhardt, J.B. Bayless, *Plasma Sources Sci. Technol.* 6 (1997) 251.
- [8] Y.H. Song, S.J. Kim, K. Choi, T. Yamamoto, *J. Electrostat.* 55 (2002) 189–201.
- [9] H.H. Kim, A. Ogata, S. Futamura, *J. Phys. D: Appl. Phys.* 38 (2005) 1292–1300.
- [10] E. Marotta, A. Callea, M. Rea, C. Paradisi, *Environ. Sci. Technol.* 41 (2007) 5862–5868.
- [11] H.L. Chen, H.M. Lee, S.H. Chen, M.B. Chang, *Ind. Eng. Chem. Res.* 47 (2008) 2122–2130.
- [12] J. Ryczkowski, *Catal. Today* 68 (2001) 263–381.
- [13] J.-S. Chang, P.A. Lawless, T. Yamamoto, *IEEE Trans. Plasma Sci.* 19 (1991) 1102–1166.
- [14] M. Kraus, B. Eliasson, U. Kogelschatz, A. Wokaun, *Phys. Chem. Chem. Phys.* 3 (2001) 294–300.
- [15] S. Imamura, M. Ikebata, T. Ito, T. Ogita, *Ind. Eng. Chem. Res.* 30 (1991) 217–221.
- [16] B. Dhandapani, S.T. Oyama, *Appl. Catal. B: Environ.* 11 (1997) 129–166.
- [17] J.V. Durme, J. Dewulf, C. Leys, H.V. Langenhove, *Appl. Catal. B: Environ.* 78 (2008) 324–333.
- [18] J.C. Whitehead, *Pure Appl. Chem.* 82 (2010) 1329–1336.
- [19] U. Diebold, *Surf. Sci. Rep.* 48 (2003) 53–229.
- [20] O. Carp, C.L. Huisman, A. Reller, *Prog. Sol. State Chem.* 32 (2004) 33–177.
- [21] R.M. Alberici, W.F. Jardim, *Appl. Catal. B: Environ.* 14 (1997) 55–68.
- [22] O. Guaitella, F. Thevenet, E. Puzenat, C. Guillard, A. Rousseau, *Appl. Catal. B: Environ.* 80 (2008) 296–305.
- [23] F. Arsac, D. Bianchi, J.M. Chovelon, C. Ferronato, J.M. Hermann, *J. Phys. Chem. A* 110 (2006) 4202–4212.
- [24] F. Arsac, D. Bianchi, J.M. Chovelon, C. Ferronato, J.M. Hermann, *J. Phys. Chem. A* 110 (2006) 4213–4222.
- [25] S.A. Larson, J.A. Widgren, J.L. Falconer, *J. Catal.* 157 (1995) 611–625.
- [26] W. Xu, D. Raftery, J.S. Fransisco, *J. Phys. Chem. B* 107 (2003) 4537–4544.
- [27] L. Sivachandiran, F. Thevenet, P. Gravejat, A. Rousseau, *Chem. Eng. J.* 214 (2013) 17–26.
- [28] U. Kogelschatz, B. Eliasson, M. Hirth, *Ozone Sci. Eng.* 10 (1988) 367–378.
- [29] T.C. Manley, *Trans. Electrochem. Soc.* 84 (1943) 83–96.
- [30] Z. Falkenstein, J.J. Coogan, *J. Phys. D: Appl. Phys.* 30 (1997) 817–825.
- [31] J.P. Coates, in: R.A. Meyers (Ed.), *Encyclopedia of Analytical Chemistry*, J. Wiley & Sons, Ltd., Chichester, UK, 2000, pp. 10815–10837.
- [32] C.-P. Sherman Hsu, *Handbook of Instrumental Techniques for Analytical Chemistry*, Prentice-Hall, Inc., Upper Saddle River, New Jersey, 1997, pp. 247–283 (Chapter 15).
- [33] T. Armoli, T. Bécue, S. Gautier, *Oil Gas Sci. Technol. – Rev. IFP* 59 (2004) 215–237.
- [34] F.C. Meunier, A. Goguet, C. Hardacre, R. Burcha, D. Thompsett, *J. Catal.* 252 (2007) 18–22.
- [35] J. Couple, P. Gravejat, F. Gaillard, D. Bianchi, *Appl. Catal. A: Gen.* 371 (2009) 99–107.
- [36] M. El-Maazawi, A.N. Finken, A.B. Nair, V.H. Grassian, *J. Catal.* 191 (2000) 138–146.
- [37] P.F. Rossi, G. Busca, V. Lorenzelli, O. Saur, J.C. Lavalle, *Langmuir* 3 (1987) 52–58.
- [38] K.M. Bulanin, J.C. lavalley, A.A. Tsyganenko, *J. Phys. Chem.* 99 (1995) 10294–10298.
- [39] J. Araña, A.P. Alonso, J.M.D. Rodríguez, G. Colón, J.A. Navío, J.P. Peña, *Appl. Catal. B: Environ.* 89 (2009) 204–213.
- [40] J.M. Coronado, S. Kataoka, I. Tejedor-Tejedor, M.A. Anderson, *J. Catal.* 219 (2003) 219–230.
- [41] L.-F. Liao, W.-C. Wu, C.-Y. Chen, J.-L. Lin, *J. Phys. Chem. B* 105 (2001) 7678–7685.